
Astronomical and atmospheric impacts on deep-sea hydrothermal vent invertebrates

Lelièvre Yann ^{1,2,*}, Legendre Pierre ², Matabos Marjolaine ¹, Mihály Steven ³, Lee Raymond W. ⁴, Sarradin Pierre-Marie ⁵, Arango Claudia P. ¹, Sarrazin Jozée ¹

¹ Ifremer Centre de Bretagne, REM/EEP, Laboratoire Environnement Profond, 29280 Plouzané, France

² Département de sciences biologiques, Université de Montréal, C.P. 6128, succursale Centre-ville, Montréal, Québec, Canada

³ Ocean Networks Canada, University of Victoria, PO Box 1700 STN CSC, Victoria, British Columbia, Canada

⁴ School of Biological Sciences, Washington State University, Pullman, WA 99164, USA

⁵ Biodiversity Program, Queensland Museum, PO BOX 3300, South Brisbane, Queensland 4101, Australia

* Corresponding author : Yann Lelièvre, email address : yann.lelievre@ifremer.fr

Abstract :

Ocean tides and winter surface storms are among the main factors driving the dynamics and spatial structure of marine coastal species, but the understanding of their impact on deep-sea and hydrothermal vent communities is still limited. Multidisciplinary deep-sea observatories offer an essential tool to study behavioural rhythms and interactions between hydrothermal community dynamics and environmental fluctuations. Here, we investigated whether species associated with a *Ridgeia piscesae* tubeworm vent assemblage respond to local ocean dynamics. By tracking variations in vent macrofaunal abundance at different temporal scales, we provide the first evidence that tides and winter surface storms influence the distribution patterns of mobile and non-symbiotic hydrothermal species (i.e. pycnogonids *Sericosura* sp. and Polynoidae polychaetes) at more than 2 km depth. Local ocean dynamics affected the mixing between hydrothermal fluid inputs and surrounding seawater, modifying the environmental conditions in vent habitats. We suggest that hydrothermal species respond to these habitat modifications by adjusting their behaviour to ensure optimal living conditions. This behaviour may reflect a specific adaptation of vent species to their highly variable habitat.

Keywords : Deep-sea observatory, hydrothermal vents, macrofaunal abundance, surface, storms, tides, time-series analyses, behavior rhythms.

64 **1. INTRODUCTION**

65 Benthic communities associated with hydrothermal vents have been extensively studied since
66 their discovery in 1977 on the Galápagos ridge [1]. Vent communities, based on local
67 chemosynthetic microbial production, are characterized by low diversity, large biomass and
68 high level of endemic species [2]. Dependent on fluid emissions, hydrothermal species are
69 distributed along an environmental gradient created by the mixing of hot hydrothermal fluids
70 (up to 400 °C) with cold surrounding seawater (<2 °C). Within a single vent site, the high
71 spatial and temporal variability of vent emissions creates a mosaic of habitats characterized
72 by contrasted physical and chemical conditions [3]. The spatial distribution of species results
73 from an interplay between their physiological tolerances to environmental conditions [4–6],
74 resource availability [7,8] and biotic factors [9,10]. Because of their unstable nature, temporal
75 and spatial components of environmental variability play a key role in the functioning of these
76 ecosystems. The diversity and structure of vent communities evolves at different scales in
77 response to the gradient of hydrothermal fluids, which control the successional dynamics of
78 communities [11–13]. Numerous studies also stressed the importance of biological
79 interactions such as predation [9,14], competition [7,9], facilitation [10,15] and inhibition
80 [10,16] on the structure and succession of vent communities.

81

82 Hydrothermal ecosystems are variable along a spatial (from cm to hundreds of km) and
83 temporal (from seconds to years) continuum. At broad spatial and temporal scales, the
84 stability of hydrothermal activity and site life span are linked to geodynamic processes such
85 as tectonic or volcanic events [17,18], that can cause important physical, chemical and
86 biological changes [19,20]. At the meter scale, mixing of hydrothermal fluids with seawater
87 creates narrow gradients of environmental conditions [21,22]. Finally, on short temporal
88 scales, high fluctuations of temperature and chemical conditions result from turbulent mixing
89 of hydrothermal fluids and ambient seawater, that are influenced both by variability in
90 hydrothermal fluid flux and local oceanic currents. These deep-sea currents can be forced
91 both astronomically through the periodic variability of surface tides [23–25], and
92 atmospherically by the passage of storms [25,26].

93

94 Ocean tides are one of the most important factors controlling intertidal communities [27] but
95 their action on deep-sea communities is less understood. Several studies have shown that
96 physical and chemical conditions in hydrothermal habitats are strongly affected by the tide in
97 the Atlantic [28–30] and Pacific ocean [23,24,31]. Two mechanisms can explain this tidal

98 influence on the hydrothermal environment. (i) The modulation of the thickness of the
99 thermal boundary created by the interaction of vent effluent and ambient seawater layer by
100 tidal currents. (ii) Direct influence of hydrothermal effluent flux by the effect of pressure of
101 sea-surface and Earth tides on the poro-elasticity of the oceanic crust [23,29]. In addition,
102 winter storms affect bottom currents by generating downward propagating inertial waves and
103 low-frequency currents generated by the pressure fluctuation associated with their passage
104 [32,33].

105

106 Tides may impact faunal distribution by altering the nature and composition of hydrothermal
107 fluids [34–36], but few studies have managed to confirm these hypotheses due to the
108 difficulty of acquiring high-resolution temporal data. To our knowledge, tide influence has
109 only been detected on two symbiotic taxa structuring hydrothermal ecosystems, with: (i) an
110 effect on *Bathymodiolus sp.* (Mytilidae, Bivalvia) growth rates [34,37,38] and (ii) an impact
111 on *Ridgeia piscesae* (Siboglinidae, Polychaeta) branchial plume movements [36]. Their
112 response to tidal cycles could reflect the variability of seawater mixing with vent fluids,
113 which directly influence the availability of oxygen and energy resources for their symbionts
114 [4].

115

116 Understanding precisely how environmental variability influences vent community dynamics
117 is of particular relevance for hydrothermal biology. To date, only a few studies describing
118 how the activity of vent fauna varies at high frequencies have been published [35,36]. To
119 establish whether the tide plays a role in vent species distributions, the variability of
120 macrofaunal abundance in a *Ridgeia piscesae* siboglinid assemblage from a northeast Pacific
121 hydrothermal edifice was investigated at high temporal resolution. The recent development of
122 deep-sea observatories has allowed for high-resolution *in situ* studies of benthic communities
123 [35,36,39,40]. Video imagery proved to be a good means of studying community dynamics
124 and behaviour [40,41], as well as small-scale changes in activity and faunal distribution
125 [35,36]. This non-invasive method allows for direct observations and provides information on
126 organisms in their natural environment [42]. Since 2009, the Ocean Networks Canada's
127 (ONC's) observatory has provided continuous power and communication to instruments
128 deployed on the seafloor. One of the instrumented arrays is located on the Main Endeavour
129 Field (Endeavour Segment, Juan de Fuca Ridge) and hosts the TEMPO-mini ecological
130 module [43], located on the Grotto edifice (Fig. 1ABC).

131

132 Based on previous observations [36], we hypothesized that the fauna associated to *Ridgeia*
133 *piscisae* tubeworms might respond to the tidal signal in response to changes in food
134 availability and environmental conditions. The objectives of the present study are to (i)
135 measure environmental conditions in relation to atmospheric and astronomic forcing, (ii)
136 determine if species associated with the *R. piscisae* assemblage respond to these forces and
137 (iii) assess changes in species activity in relation to variations in environmental conditions.

138

139 **2. MATERIAL AND METHODS**

140 *(a) Study site*

141 The 90-km Endeavour segment located on the northern part of the Juan de Fuca Ridge
142 (JdFR), hosts 5 major hydrothermal vent fields concentrated within a 1-km-wide, 10-km-long
143 rift valley located along the ridge crest [44]. Within the Main Endeavour Field (Fig. 1A),
144 Grotto (47°56.958'N, 129°5.899'W) is a hydrothermal sulphide vent cluster (area ~450 m²)
145 that forms a cove opened to the north (Fig. 1B), and is one of the most hydrothermally active
146 structures in the Main Endeavour Field [45].

147

148 *(b) TEMPO-mini ecological observatory module*

149 TEMPO-mini [43] is deployed on the north slope of the Grotto edifice at 2 196 m depth (Fig.
150 1C) on ONC's NEPTUNE observatory Endeavour node. The module is equipped with an
151 Axis Q1755 camera, four 20W LED lights, an Aanderaa optode coupled with a temperature
152 probe, a 10 m thermistor chain (T-chain) and a CHEMINI chemical analyzer (not installed
153 during our study). The camera and projectors are protected against biofouling by localized
154 microchloration [46]. To study long-term temporal dynamics of vent communities, the camera
155 was programmed to record 20-min video sequences six times a day (at 02 h, 06 h, 10 h, 14 h,
156 18 h and 22 h UTC) with three zoom changes: "Large", "Medium" and "Fine" views. The
157 camera was focused on a *Ridgeia piscisae* tubeworm assemblage harbouring a dense
158 community of associated fauna. The total studied surface covers approximately 0.315 m². In
159 the absence of a 3D model, the observation area was considered to form a two-dimensional
160 surface.

161

162 *(c) Environmental characterization*

163 Pressure, currents, temperature and oxygen were acquired by instruments installed on or near
164 Grotto (Fig. 1C). Pressure and currents were measured with a highly sensitive bottom

165 pressure recorder (BPR) and a 600 KHz acoustic Doppler current meter (ADCP) with a useful
166 vertical range of about 30 m, located about 70 m south of Grotto in a flat area without
167 hydrothermal activity. Temperatures were measured by: (i) a 25 cm long thermocouple wand
168 (BARS) inserted into a vigorously venting black smoker orifice located about 10 m west of
169 TEMPO-mini, (ii) twelve autonomous temperature loggers (F-probes; F1-F12) placed on a
170 tubeworm assemblage, (iii) the Aanderaa oxygen sensor deployed 30 to 40 cm below the field
171 of view and (iv) a probe located under a fluid-collection benthic chamber of the remote access
172 fluid sampler (RAS) from a nearby (~1.5 m) diffuse venting area. Oxygen saturation was
173 measured by the Aanderaa optode (see Table S1).

174

175 In order to investigate the seasonal component of storms activity in the northeast Pacific
176 Ocean, surface wind stresses (horizontal force of the wind on the sea surface) and wave
177 heights were used as indicators of storm's activity. Data come from a meteorological buoy
178 called "Station 46206 - La Perouse Bank" (48.835 N, 125.998 W; Environnement Canada)
179 located 70 km off the west coast of Vancouver Island. The atmospheric forcing has typical
180 scales of hundreds to thousands of kilometers. Consequently, measurements of winds stress
181 and wave heights by the meteorological buoy are thus a signature of climate variability not
182 only over the local site, but also in the northeast Pacific Ocean.

183

184 *(d) Observation design*

185 Temporal variations in observed abundances of four taxa (Ammotheidae, Polynoidae,
186 Buccinidae and Zoarcidae) were quantified using large and medium views. To avoid observer
187 bias among consecutive measurements, video sequences were analysed in random order. The
188 first observation strategy had a fixed daily observation time set at 10:00 UTC encompassing a
189 year from 2013-06-20 to 2014-06-20. The second observation strategy was designed to
190 identify seasonal components of macrofaunal and environmental variability. Six observations
191 per day (02:00, 06:00, 10:00, 14:00, 18:00 and 22:00 UTC) were conducted in one summer
192 (June 2014) and two winter (November and December, 2014) months. The selection of these
193 periods was performed in order to minimize the amount of missing data and promote the
194 presence of high-quality video imagery.

195

196 *(e) Statistical methods*

197 For environmental variables, Welch's averaged modified periodogram method [47,48] was

198 used to identify the dominant periods, and tidal harmonic analysis using open source program
199 t-tide [49] was used to assess the timing (phase of the cycles) and the degree to which the
200 periodicities were determined by tidal forcing. Prior to analysis, the two-dimensional currents
201 were rotated into components along and across the axis of the ridge. The spectra of the
202 currents from fourteen depth ranges from 4 m to 30 m above bottom were examined.

203

204 After substituting missing values using a k-nearest neighbours method in the more sparsely
205 observed macrofaunal abundances time series, Dutilleul's multi-frequential periodogram
206 analysis (MFPA) was used to identify dominant periods [50]. This periodogram computes the
207 variance of periods that do not correspond to an integer number of cycles (fractional
208 frequencies) by the regression on to the sinusoidal representation of the considered frequency.
209 The statistic of Dutilleul's periodogram is defined as the fraction of the total variance of the
210 time series explained by regressing this series on the cosine and sine corresponding to the
211 considered frequency; p-value are produced.

212

213 Using *Piste 3.2.1* (Legendre laboratory, Université de Montréal), path analyses [51] were
214 performed on monthly analyses to investigate how tides affect the variability of macrofaunal
215 abundance. We based the conceptual structure of the path model (Fig. 3) on the hypotheses
216 that near bottom currents influences local environmental conditions (measured variables:
217 temperature and oxygen saturation), that both jointly influence macrofaunal abundance. Thus,
218 the path model had multiple intermediate levels: (i) hydrodynamic processes were defined by
219 axial currents, (ii) seawater and hydrothermal fluid mixing defined by temperature from the F-
220 probe contributing the most to explaining faunal variability and the single oxygen sensor, and
221 (iii) faunal abundance.

222

223 **3. RESULTS AND DISCUSSION**

224 Ocean tides and surface storms are the main drivers of ocean dynamics [23,26]. These
225 processes create temporal hydrodynamic patterns at different frequencies, which influence the
226 marine ecosystems from coastal zones down to abyssal environment. Using deep-sea cabled
227 observatory approach, we found that the physical and chemical environment of Grotto
228 hydrothermal edifice is strongly influenced by hydrodynamic processes, suggesting a possible
229 influence on vent fauna. Behavioural rhythms studies are essential to understand how species
230 interact with their environment. Widely studied in coastal species, the presence of these
231 rhythms in benthic fauna remains largely unknown [57,58]. A multi-frequential periodogram

232 analysis computed on observed abundance time series revealed that Ammotheidae
233 pycnogonid and Polynoidae polychaete respond to tides and surface storms. Here, we show
234 for the first time a significantly influence of hydrodynamic processes on distribution patterns
235 of mobile and non-symbiotic hydrothermal species at >2 km depth.

236

237 *Environmental conditions and ocean dynamics*

238 Most of the environmental measurements were obtained in close proximity to the video-
239 analysed siboglinid assemblage using the cabled instruments of ONC's NEPTUNE
240 observatory (Fig. 1C). Environmental conditions over the study period are summarized in
241 Table S1. Spectral analysis showed that bottom pressure was dominated by peaks in energy
242 centred near frequencies of 1 and 2 cycles per day, the diurnal (12.4 h) and semidiurnal tidal
243 bands (24.8 h) (Fig. 2). The ratio of energy between the near-semidiurnal and near-diurnal
244 bands matched those of barotropic tidal models of the northeast Pacific [52,53] with the near-
245 semidiurnal band being about twice as energetic as the near-diurnal. Similarly, the dominant
246 peak in the current spectra were in the diurnal and semidiurnal bands with the near-
247 semidiurnal band being five times more energetic than the near-diurnal band (Fig. 2).
248 Harmonic analyses of the pressure and current time series revealed that the tidal constituents
249 accounted for 99% and 31% of the variance, respectively. In both instances, the dominant
250 constituent of the near-semidiurnal band was the principal lunar tidal constituent, M_2 , at a
251 period of 12.42 h [25], which had three times the amplitude of the second dominant
252 constituent, the principal solar semidiurnal, S_2 at 12 h. In the near-diurnal band, the lunar
253 diurnal constituent K_1 (23.93 h) in both pressure series dominated the solar diurnal constituent
254 P_1 (24.07 h) by a factor of 2.5. We also observed an enhanced energy peak at a 3 to 4 day
255 period and at higher nonlinear harmonics of the tidal frequencies. The shape of the spectrum
256 of currents observed at 4 m above the bottom (mab) through those observed at 30 mab was
257 very similar; however, the total spectral energy increased away from the seafloor by a factor
258 of two from the bottom (4 mab) to the top (30 mab) measurements in the water column.
259 Notable is that the semidiurnal energy was almost entirely concentrated in the along-valley
260 axis component and greatly diminished in the weak cross-axis component (data not shown).
261 The spectra of temperatures and oxygen saturation from a diffuse venting area obtained from
262 the F-probes and Aanderaa optode also revealed significant peaks at the near-semidiurnal and
263 near-diurnal frequencies (Fig. 2). These tidal peaks had less power than those of the pressure
264 and current spectra. Higher nonlinear harmonics of these fundamental tidal peaks were found
265 to varying degrees in several of the spectra. Tidal oscillations were more episodic and less

266 persistent in diffuse fluids than in the high-temperature black smoker fluids, where tidal
267 oscillations were more steady and comparable to the pressure record.

268

269 Looking at the phase relationship among the environmental variables, tidal pressures at Grotto
270 were inversely related to temperature variations of the monitored black smoker. The predicted
271 tide from the pressure and high-temperature time series showed that the end-member (pure
272 hydrothermal) fluid temperature was lower during periods of higher tidal pressure (Fig. S1).
273 Presuming that the change in pressure due to tides forces the change in temperature [54], the
274 phase angle of the dominant predicted tide (M_2 constituent) can be used to estimate the
275 pressure-temperature lag, which at our high-temperature site would be approximately 213° .
276 At the M_2 tidal frequency, this phase lag is about 7.3 h.

277

278 Ambient currents have a complex but direct control on temperature variability in diffuse
279 venting areas and these variations in temperature can be a proxy measurement of the chemical
280 variability of the hydrothermal fluids [55,56]. Since within the rift valley, the dominant
281 periodicity of ambient currents is tidal, we can expect a strong tidal effect on the environment
282 surrounding the faunal community.

283

284 *Impacts of ocean tides on hydrothermal ecosystems*

285 The temporal variability in hydrothermal macrofaunal communities was evaluated in relation
286 to tidal action in the Endeavour rift valley. Dutilleul's periodograms computed on one year of
287 simulated data showed that, with one observation per day, a cosine with 12.4 h tidal period
288 produces a 15-day harmonic. This 15-day period was detected on the observed abundances of
289 Ammotheidae pycnogonids (Table S2), highlighting a tidal signal. For the June, November
290 and December 2014 time series (6 observations per day), periodograms also displayed a
291 significant 12.4 h period corresponding to the semidiurnal tide cycle (Table S2). The observed
292 abundances of Polynoidae polychaetes at the top of the *Ridgeia* bush exhibited a significant
293 tidal cycle (12.4 h) only during the December month (Table S2). Periodograms on Zoarcidae
294 fish abundances did not highlight any significant tide-related periodicity (Table S2).
295 Likewise, periodograms computed on Buccinidae gastropod activity revealed no specific
296 relationship with the tidal signal (Table S2). Successful detection of tidal signals in observed
297 species abundances depends upon the studied time interval, the observation frequency, as well
298 as the abundance and behaviour of the faunal species. When a species is abundant the
299 observer errors causes negligible effects on the observed variability. In contrast, a taxa

300 represented by a small number of individuals is less likely to display a statistically significant
301 relationship because observer errors increase the variance, creating noise in abundance data.
302 The low number of individuals, combined with the reduced mobility for buccinids, may
303 explain the absence of significant periodicity. Stochastic events (tectonic, volcanic or food
304 inputs), which are common in hydrothermal vents, may also mask an underlying rhythmicity
305 if the response of species to these events is stronger than it is to tides, by generating
306 irregularity in regular biological cycles [59]. Finally, the abundance variations of some taxa
307 might just not be influenced by the tides and associated environmental conditions.

308

309 To deepen our understanding of tide-related impacts, we decomposed their relationship with
310 the temporal dynamics of vent macrofaunal communities using path analyses performed on
311 one-month observation periods (Fig. 3). For all the months studied, path analysis results
312 highlighted a strong influence of northern and southern horizontal bottom currents (along-axis
313 currents) on the local physical and chemical conditions of tubeworms habitat. These currents
314 had a strong negative effect on temperature and a strong positive effect on oxygen (Fig. 3).
315 The high influence of northern and southern horizontal bottom currents (valley axis) on local
316 environmental conditions is in concordance with the main orientation of the ridge and
317 topography of the Grotto site. The horseshoe-shaped hydrothermal cluster is opened on the
318 northeast side, directly exposed to north-south current axis (Fig. 1B). The height of the
319 northern towers (10 m) may further protect the assemblage from east/west currents. The tidal
320 modulation of bottom currents is reflected in the fluctuation of current velocities and
321 direction, influencing diffuse flow mixing plumes and therefore, local environmental
322 gradients (Scheirer *et al.* 2006). We show that the tidal forcing causes environmental
323 conditions to alternate between two regimes, which in turn significantly affects the tubeworm
324 assemblage. In particular, the siboglinid habitat fluctuates between warm-low oxygen and
325 cool-high oxygen periods. Temperature is one of the main drivers of vent species distributions
326 and a proxy to trace the turbulent mixing between hot hydrothermal fluids and cold seawater
327 [22,56]. Generally, higher hydrothermal fluid inputs lead to the presence of higher
328 concentrations of hydrogen sulphide and other reduced chemicals (methane, sulphur, metals,
329 etc.) as well as a lower oxygen availability for communities.

330

331 Path analyses highlighted a relationship between ocean tides and macrofaunal abundance
332 through the modulation of temperature and oxygen availability by tidal currents (Fig. 3).
333 Highest species abundances were observed during northern current phases (directed to the

334 south) while southern current phases (directed to the north) were characterized by lower
335 faunal abundances. On the environmental side, the F-probes deployed on the tubeworm
336 assemblage showed that southern current phases were characterised by lower temperatures,
337 hence lower concentrations of hydrogen sulphide and higher oxygen saturation. In these
338 favourable conditions, we hypothesize that species would migrate deeper in the tubeworm
339 bush, protecting themselves against currents and predation, and possibly allocating their
340 energy to other activities such as nutrition and/or reproduction (Fig. 4). Individuals within the
341 tubeworm bush were not visible to the observer, reducing the number of counted individuals.
342 Conversely, the northern current phases were associated with higher temperatures and low
343 oxygen saturation, suggesting higher inputs of hydrothermal fluids in the habitat. We
344 postulate that vent species come to the surface of the tubeworm assemblage in search of more
345 favourable habitat conditions such as higher oxygen saturation (Fig. 4).

346

347 Aggregation and enhanced activity of pycnogonids occurred during higher temperature and
348 lower oxygen saturation periods. In the reverse conditions, pycnogonids were fewer and less
349 active, rendering observations more difficult. This behaviour could be associated to the
350 respiration. In the absence of a respiratory system and pigments that can transport oxygen
351 [60,61], pycnogonids breathe through their exoskeleton by diffusion [62]. Since their cardiac
352 system is too weak to circulate the hemolymph [63], leg joint and peristaltic movements exert
353 pressure on the hemolymph, allowing the oxygen transport [64,65]. Oxygen consumption
354 varies with their activity levels but also with the number of individuals present [66]. Indeed,
355 oxygen consumption is influenced by individuals touching one another and respiration
356 appears to be greater when pycnogonids gather than when they are isolated [66].

357

358 The two endemic polynoid polychaete taxa of the Endeavour vent field (*Branchinotogluma*
359 *sp.* and *Lepidonotopodium piscisae*) showed no distinctive pattern in abundance in relation to
360 tides. Hydrothermal polynoids tolerate a wide range of thermal conditions and the absence of
361 significant influence of temperature on their abundance is in agreement with previous findings
362 that these two species are found within their thermal optimal range [41,67]. In contrast with
363 littoral species, the presence of gills and hemoglobins with high affinity for oxygen in vent
364 polynoids promote oxygen uptake in such hypoxic environments. However, in December
365 2014, polynoid abundance pattern followed a tidal signal in relation with currents. These
366 currents might modulate the availability of food or/and other unmeasured environmental
367 variables but the occurrence of this signal only in December remains to be investigated.

368

369 *Influence of surface storms on deep-sea fauna*

370 Atmospheric forcing exerts a strong influence on surface ocean dynamics whose effects
371 propagate down to hydrothermal ecosystems. Wind stress and wave height components were
372 plotted for 2014 in order to highlight a seasonal component in storm activity of the northeast
373 Pacific Ocean (Fig. 5). In the summer, wave height is relatively low which is consistent with
374 the reduced wind stresses. However, winter season show a greater instability and suggests an
375 increase of storms activity in the northeast Pacific (Fig. 5).

376

377 Ammotheidae and Polynoidae observed abundances responded to local atmospheric forcing
378 with a 4-day oscillation and 16 h inertial oscillation respectively, possibly related to surface
379 storms (Table S2). Evidence of 4-day storm-related oscillations in currents and hydrothermal
380 effluents has been previously reported along the Juan de Fuca Ridge [26,68] and is present in
381 our pressure and current spectra (Fig 2). At the latitude of our study site, the 16 h period
382 corresponds to that of wind-generated inertial currents. When winds at the sea surface are
383 weak or absent, previously induced water movements trace inertia circles because of the
384 Coriolis effect due to the Earth's rotation. Induction of these initial movements may be caused
385 by the passage of storms. This period was previously observed in the times series of Grotto
386 hydrothermal fluxes, showing an influence of surface storms on the dynamics of
387 hydrothermal plumes [69]. However, the environmental variable spectra (Fig. 2) within the
388 rift valley do not reveal significant energy at the 16 h inertial period and we postulate that the
389 narrowness and small size of the rift valley may not permit the entry of internal inertial
390 waves, which are large and propagate at a very small (< 2 deg) angle to the horizontal plane.
391 Conversely, these inertial waves are enhanced above the ridge (~ 200 mab) [25] where they
392 can periodically advect the neutrally buoyant vent plume and its resident particles. Thus, we
393 postulate that the 4-day oscillations and inertial period (16 h) could be impressed upon the
394 faunal activity by the periodic variability of local environmental conditions and particles
395 settling from the hydrothermal plumes (Fig. 4).

396

397 **5. CONCLUSION**

398 The influence of astronomical and atmospheric forcing on the ocean generates temporal
399 hydrodynamic patterns whose signatures are found in hydrothermal ecosystems. This study
400 showed for the first time a response of observed abundances of non-symbiotic vent species to

401 the tidal cycle. Our results also revealed an influence of ocean surface storm periodicities
402 during the winter months. These patterns were controlled by near-bottom current variability,
403 which modulates habitat conditions and indirectly influences faunal dynamics. It is now clear
404 that surface ocean dynamics plays a significant role in the functioning of hydrothermal
405 ecosystems.

406

407 An alternative assumption would be the presence of endogenous timekeeping mechanisms,
408 the so-called biological clock. Encoded by clock genes [70], biological rhythms are
409 phylogenetically constrained without being necessarily linked with the presence of cyclic
410 environmental signals. An emerging literature on these endogenous rhythms in deep-sea
411 species suggests an important role of tides in species activity [36,39,58]. Biological rhythms
412 could constitute an anticipated response of organisms to changing environmental conditions
413 caused by ocean variability. In order to test these assumptions, *in vivo* experiments in
414 pressurised aquariums should be investigated.

415

416 REFERENCES

- 417 1. Lonsdale, P. 1977 Clustering of suspension-feeding macrobenthos near abyssal
418 hydrothermal vents at oceanic spreading centers. *Deep. Res. Part I Oceanogr. Res.*
419 *Pap.* **24**, 857–863.
- 420 2. Tunnicliffe, V. 1991 The biology of hydrothermal vents: ecology and evolution.
421 *Oceanogr. Mar. Biol. Annu. Rev.* **29**, 319–407.
- 422 3. Sarradin, P.-M., Caprais, J.-C., Briand, P., Gaill, F., Shillito, B. & Desbruyères, D.
423 1998 Chemical and thermal description of the Genesis hydrothermal vent community
424 environment (13°N, EPR). *Cah. Biol. Mar.* **39**, 159–167.
- 425 4. Childress, J. J. & Fisher, C. R. 1992 The biology of hydrothermal vent animals:
426 physiology, biochemistry, and autotrophic symbioses. *Oceanogr. Mar. Biol. Annu. Rev.*
427 **30**, 337–441.
- 428 5. Sarrazin, J., Juniper, S. K., Massoth, G. & Legendre, P. 1999 Physical and chemical
429 factors influencing species distributions on hydrothermal sulfide edifices of the Juan de
430 Fuca Ridge, northeast Pacific. *Mar. Ecol. Prog. Ser.* **190**, 89–112.
431 (doi:10.3354/meps190089)
- 432 6. Luther, G., Rozan, T., Taillefert, M., Nuzzio, D., Di Meo, C., Shank, T., Lutz, R. &
433 Cary, C. 2001 Chemical speciation drives hydrothermal vent ecology. *Nature* **410**,
434 813–816. (doi:10.1038/35071069)
- 435 7. Levesque, C., Juniper, S. K. & Marcus, J. 2003 Food resource partitioning and

- 436 competition among alvinellid polychaetes of Juan de Fuca Ridge hydrothermal vents.
437 *Mar. Ecol. Prog. Ser.* **246**, 173–182. (doi:10.3354/meps246173)
- 438 8. De Busserolles, F., Sarrazin, J., Gauthier, O., Gélinas, Y., Fabri, M.-C., Sarradin, P.-M.
439 & Desbruyères, D. 2009 Are spatial variations in the diets of hydrothermal fauna
440 linked to local environmental conditions? *Deep. Res. Part II Top. Stud. Oceanogr.* **56**,
441 1649–1664. (doi:10.1016/j.dsr2.2009.05.011)
- 442 9. Micheli, F., Peterson, C. H., Mullineaux, L. S., Fisher, C. R., Mills, S. W., Sancho, G.,
443 Johnson, G. a. & Lenihan, H. S. 2002 Predation structures communities at deep-sea
444 hydrothermal vents. *Ecol. Monogr.* **72**, 365–382. (doi:10.1890/0012-
445 9615(2002)072[0365:PSCADS]2.0.CO;2)
- 446 10. Mullineaux, L. S., Peterson, C. H., Micheli, F. & Mills, S. W. 2003 Successional
447 mechanism varies along a gradient in hydrothermal fluid flux at deep-sea vents. *Ecol.*
448 *Monogr.* **73**, 523–542. (doi:10.1890/02-0674)
- 449 11. Shank, T. M., Fornari, D. J., Von Damm, K. L., Lilley, M. D., Haymon, R. M. & Lutz,
450 R. A. 1998 Temporal and spatial patterns of biological community development at
451 nascent deep-sea hydrothermal vents (9°50'N, East Pacific Rise). *Deep. Res. Part II-*
452 *Topical Stud. Oceanogr.* **45**, 465–515.
- 453 12. Sarrazin, J. & Juniper, S. K. 1999 Biological characteristics of a hydrothermal edifice
454 mosaic community. *Mar. Ecol. Prog. Ser.* **185**, 1–19. (doi:10.3354/meps185001)
- 455 13. Sarrazin, J., Robigou, V., Juniper, S. K. & Delaney, J. R. 1997 Biological and
456 geological dynamics over four years on a high-temperature sulfide structure at the Juan
457 de Fuca Ridge hydrothermal observatory. *Mar. Ecol. Prog. Ser.* **153**, 5–24.
458 (doi:10.3354/meps153005)
- 459 14. Sancho, G., Fisher, C. R., Mills, S., Micheli, F., Johnson, G. a., Lenihan, H. S.,
460 Peterson, C. H. & Mullineaux, L. S. 2005 Selective predation by the zoarcid fish
461 *Thermarces cerberus* at hydrothermal vents. *Deep. Res. Part I Oceanogr. Res. Pap.* **52**,
462 837–844. (doi:10.1016/j.dsr.2004.12.002)
- 463 15. Mullineaux, L. S., Fisher, C. R., Peterson, C. H. & Schaeffer, S. W. 2000 Tubeworm
464 succession at hydrothermal vents: use of biogenic cues to reduce habitat selection
465 error? *Oecologia* **123**, 275–284. (doi:10.1007/s004420051014)
- 466 16. Lenihan, H. S., Mills, S. W., Mullineaux, L. S., Peterson, C. H., Fisher, C. R. &
467 Micheli, F. 2008 Biotic interactions at hydrothermal vents: Recruitment inhibition by
468 the mussel *Bathymodiolus thermophilus*. *Deep. Res. Part I Oceanogr. Res. Pap.* **55**,
469 1707–1717. (doi:10.1016/j.dsr.2008.07.007)
- 470 17. Fouquet, Y., Auzende, J., Ballu, V., Batiza, R., Bideau, D., Cormier, M., Geistdoerfer,
471 P., Lagabrielle, Y. & Sinton, J. 1994 Variabilité des manifestations hydrothermales
472 actuelles le long d'une dorsale ultra-rapide : exemple de la dorsale Est Pacifique entre
473 17° et 19° S (campagne NAUDUR). *Comptes Rendus l'Academie des Sci. Ser. II* **319**,
474 1399–1406.

- 475 18. Tunnicliffe, V., Embley, R. W., Holden, J. F., Butterfield, D. a., Massoth, G. J. &
476 Juniper, S. K. 1997 Biological colonization of new hydrothermal vents following an
477 eruption on Juan de Fuca Ridge. *Deep. Res. Part I Oceanogr. Res. Pap.* **44**, 1627–
478 1644. (doi:10.1016/S0967-0637(97)00041-1)
- 479 19. Juniper, S. K. & Tunnicliffe, V. 1997 Crustal accretion and the hot vent ecosystem.
480 *Philos. Trans. R. Soc. A Math. Phys. Eng. Sci.* **355**, 459–474.
481 (doi:10.1098/rsta.1997.0017)
- 482 20. Macdonald, K. C. 1998 Linkages between faulting, volcanism, hydrothermal activity
483 and segmentation on fast spreading centers. *Geophys. Monogr. Geophys. union* **106**,
484 27–58.
- 485 21. Johnson, K. S., Beehler, C. L., Sakamoto-Arnold, C. M. & Childress, J. J. 1986 In situ
486 measurements of chemical distributions in a deep-sea hydrothermal vent field. *Science*.
487 **231**, 1139–1141.
- 488 22. Johnson, K. S., Childress, J. J., Hessler, R. R., Sakamoto-Arnold, C. M. & Beehler, C.
489 L. 1988 Chemical and biological interactions in the Rose Garden hydrothermal vent
490 field, Galapagos spreading center. *Deep Sea Res. Part A. Oceanogr. Res. Pap.* **35**,
491 1723–1744. (doi:10.1016/0198-0149(88)90046-5)
- 492 23. Tivey, M., Bradley, A., Terrence, J. & Kadco, D. 2002 Insights into tide-related
493 variability at seafloor hydrothermal vents from time-series temperature measurements.
494 *Earth Planet. Sci. Lett.* **202**, 693–707. (doi:10.1016/S0012-821X(02)00801-4)
- 495 24. Scheirer, D. S., Shank, T. M. & Fornari, D. J. 2006 Temperature variations at diffuse
496 and focused flow hydrothermal vent sites along the northern East Pacific Rise.
497 *Geochemistry, Geophys. Geosystems* **7**, 1–23. (doi:10.1029/2005GC001094)
- 498 25. Thomson, R. E., Mihály, S. F., Rabinovich, A. B., McDuff, R. E., Veirs, S. R. & Stahr,
499 F. R. 2003 Constrained circulation at Endeavour ridge facilitates colonization by vent
500 larvae. *Nature* **424**, 545–549. (doi:10.1038/nature01814.)
- 501 26. Cannon, G. A. & Thomson, R. E. 1996 Characteristics of 4-day oscillations trapped by
502 the Juan de Fuca Ridge. *Geophys. Res. Lett.* **23**, 1613–1616. (doi:10.1029/96GL01370)
- 503 27. Connell, J. H. 1972 Community interactions on marine rocky intertidal shores. *Annu.*
504 *Rev. Ecol. Syst.* **3**, 169–192.
- 505 28. Sohn, R. A. 2007 Stochastic analysis of exit fluid temperature records from the active
506 TAG hydrothermal mound (Mid-Atlantic Ridge, 26°N): 2. Hidden Markov models of
507 flow episodes. *J. Geophys. Res. Solid Earth* **112**, 1–16. (doi:10.1029/2007JB004961)
- 508 29. Barreyre, T., Escartin, J., Sohn, R. A., Cannat, M., Ballu, V. & Crawford, W. C. 2014
509 Temporal variability and tidal modulation of hydrothermal exit-fluid temperatures at
510 the Lucky Strike deep-sea vent field, Mid-Atlantic Ridge. *J. Geophys. Res. Solid Earth*
511 **119**, 2543–2566. (doi:10.1002/2013JB010478.Received)
- 512 30. Kinoshita, M., Von Herzen, R. ., Matsubayashi, O. & Fujioka, K. 1998 Tidally-driven

- 513 effluent detected by long-term temperature monitoring at the TAG hydrothermal
514 mound, Mid-Atlantic Ridge. *Phys. Earth Planet. Inter.* **108**, 143–154.
515 (doi:10.1016/S0031-9201(98)00092-2)
- 516 31. Little, S. A., Stolzenbach, K. D. & Grassle, F. J. 1988 Tidal current effects on
517 temperature in diffuse hydrothermal flow: Guaymas basin. *Geophys. Res. Lett.* **15**,
518 1491–1494.
- 519 32. Thomson, R. E., Roth, S. E. & Dymond, J. 1990 Near-inertial motions over a mid-
520 ocean ridge: Effects of topography and hydrothermal plumes. *J. Geophys. Res.* **95**,
521 7261–7278. (doi:10.1029/JC095iC05p07261)
- 522 33. D’Asaro, E. A. 1995 Upper-ocean inertial currents forced by a strong storm. Part III:
523 Interaction of inertial currents and mesoscale eddies. *J. Phys. Oceanogr.* **25**, 2953–
524 2958. (doi:10.1175/1520-0485(1995)025<2953:UOICFB>2.0.CO;2)
- 525 34. Nedoncelle, K., Lartaud, F., de Rafelis, M., Boulila, S. & Le Bris, N. 2013 A new
526 method for high-resolution bivalve growth rate studies in hydrothermal environments.
527 *Mar. Biol.* **160**, 1427–1439. (doi:10.1007/s00227-013-2195-7)
- 528 35. Sarrazin, J., Cuvelier, D., Peton, L., Legendre, P. & Sarradin, P.-M. 2014 High-
529 resolution dynamics of a deep-sea hydrothermal mussel assemblage monitored by the
530 EMSO-Açores MoMAR observatory. *Deep. Res. Part I Oceanogr. Res. Pap.* **90**, 62–
531 75. (doi:10.1016/j.dsr.2014.04.004)
- 532 36. Cuvelier, D., Legendre, P., Laes, A., Sarradin, P.-M. & Sarrazin, J. 2014 Rhythms and
533 community dynamics of a hydrothermal tubeworm assemblage at main endeavour field
534 - A multidisciplinary deep-sea observatory approach. *PLoS One* **9**, e96924.
535 (doi:10.1371/journal.pone.0096924)
- 536 37. Schöne, B. R. & Giere, O. 2005 Growth increments and stable isotope variation in
537 shells of the deep-sea hydrothermal vent bivalve mollusk *Bathymodiolus brevior* from
538 the North Fiji Basin, Pacific Ocean. *Deep. Res. Part I Oceanogr. Res. Pap.* **52**, 1896–
539 1910. (doi:10.1016/j.dsr.2005.06.003)
- 540 38. Nedoncelle, K., Lartaud, F., Contreira-Pereira, L., Yücel, M., Thurnherr, A. M.,
541 Mullineaux, L. & Le Bris, N. 2015 *Bathymodiolus* growth dynamics in relation to
542 environmental fluctuations in vent habitats. *Deep Sea Res. Part I Oceanogr. Res. Pap.*
543 (doi:10.1016/j.dsr.2015.10.003)
- 544 39. Matabos, M., Bui, A. O. V., Mihály, S., Aguzzi, J., Juniper, K. & Ajayamohan, R. S.
545 2014 High-frequency study of epibenthic megafaunal community dynamics in Barkley
546 Canyon : A multi-disciplinary approach using the NEPTUNE Canada network. *J. Mar.*
547 *Syst.* **130**, 56–68. (doi:10.1016/j.jmarsys.2013.05.002)
- 548 40. Matabos, M., Piechaud, N., De Montigny, F., Sarradin, P.-M. & Sarrazin, J. 2015 The
549 VENUS cabled observatory as a method to observe fish behaviour and species
550 assemblages in a hypoxic fjord, Saanich Inlet (British Columbia, Canada). *Can. J. Fish.*
551 *Aquat. Sci.* **72**, 1–13.

- 552 41. Robert, K., Onthank, K. L., Juniper, S. K. & Lee, R. W. 2012 Small-scale thermal
553 responses of hydrothermal vent polynoid polychaetes: Preliminary in situ experiments
554 and methodological development. *J. Exp. Mar. Bio. Ecol.* **420-421**, 69–76.
555 (doi:10.1016/j.jembe.2012.03.019)
- 556 42. Cuvelier, D., de Busserolles, F., Lavaud, R., Floc'h, E., Fabri, M.-C., Sarradin, P. M. &
557 Sarrazin, J. 2012 Biological data extraction from imagery - How far can we go? A case
558 study from the Mid-Atlantic Ridge. *Mar. Environ. Res.* **82**, 15–27.
559 (doi:10.1016/j.marenvres.2012.09.001)
- 560 43. Auffret, Y. et al. 2009 Tempo-Mini: A Custom-designed instrument for real-time
561 monitoring of hydrothermal vent ecosystems.
- 562 44. Kelley, D. S. et al. 2012 Endeavour Segment of the Juan de Fuca Ridge: one of the
563 most remarkable places on earth. *Oceanography* **25**, 44–61.
- 564 45. Xu, G., Jackson, D. R., Bemis, K. G. & Rona, P. A. 2014 Time-series measurement of
565 hydrothermal heat flux at the Grotto mound, Endeavour Segment, Juan de Fuca Ridge.
566 *Earth Planet. Sci. Lett.* **404**, 220–231. (doi:10.1016/j.epsl.2014.07.040)
- 567 46. Delauney, L., Compare, C. & Lehaitre, M. 2010 Biofouling protection for marine
568 environmental sensors. *Ocean Sci.* **6**, 503–511. (doi:10.5194/os-6-503-2010)
- 569 47. Welch, P. D. 1967 The use of fast Fourier transform for the estimation of power
570 spectra: a method based on time averaging over short, modified periodograms. *IEEE*
571 *Trans Audio AU-15*, 70–73.
- 572 48. Thomson, R. E. & Emery, W. J. 2014 *Data Analysis Methods in Physical*
573 *Oceanography*. Waltham, MA: Elsevier Science.
- 574 49. Pawlowicz, R., Beardsley, B. & Lentz, S. 2002 Classical tidal harmonic analysis
575 including werror estimates in MATLAB using T_TIDE. *Comput. Geosci.* **28**, 929–937.
576 (doi:10.1016/S0098-3004(02)00013-4)
- 577 50. Dutilleul, P. 2001 Multi-Frequential Periodogram Analysis and the detection of
578 periodic components in time series. *Commun. Stat. - Theory Methods* **30**, 1063–1098.
579 (doi:10.1081/STA-100104350)
- 580 51. Wright, S. 1934 The method of path coefficients. *Ann. Math. Stat.* **5**, 161–215.
- 581 52. Flather, R. A. 1987 A tidal model of the northeast pacific. *Atmosphere-Ocean* **25**, 22–
582 45. (doi:10.1080/07055900.1987.9649262)
- 583 53. Foreman, M. G. G., Crawford, W. R., Cherniawsky, J. Y., Henry, R. F. & Tarbotton,
584 M. R. 2000 A high-resolution assimilating tidal model for the northeast Pacific Ocean.
585 *J. Geophys. Res.* **105**, 28629. (doi:10.1029/1999JC000122)
- 586 54. Jupp, T. E. & Schultz, A. 2004 A poroelastic model for the tidal modulation of seafloor
587 hydrothermal systems. *J. Geophys. Res.* **109**, 1–14. (doi:10.1029/2003JB002583)
- 588 55. Johnson, K. S., Childress, J. J. & Beehler, C. L. 1988 Short-term temperature
589 variability in the Rose Garden hydrothermal vent field : an unstable deep-sea

- 590 environment. *Deep Sea Res. Part A. Oceanogr. Res. Pap.* **35**, 1711–1721.
- 591 56. Le Bris, N., Rodier, P., Sarradin, P.-M. & Le Gall, C. 2006 Is temperature a good
592 proxy for sulfide in hydrothermal vent habitats? *Cah. Biol. Mar.* **47**, 465–470.
- 593 57. Aguzzi, J., Costa, C., Furushima, Y., Chiesa, J. J., Company, J. B., Menesatti, P.,
594 Iwase, R. & Fujiwara, Y. 2010 Behavioral rhythms of hydrocarbon seep fauna in
595 relation to internal tides. *Mar. Ecol. Prog. Ser.* **418**, 47–56.
- 596 58. Aguzzi, J., Company, J. B., Costa, C., Menesatti, P., Garcia, J. A., Bahamon, N., Puig,
597 P. & Sarda, F. 2011 Activity rhythms in the deep-sea: a chronobiological approach.
598 *Front. Biosci.* **16**, 131–150.
- 599 59. Matabos, M., Aguzzi, J., Robert, K., Costa, C., Menesatti, P., Company, J. B. &
600 Juniper, S. K. 2011 Multi-parametric study of behavioural modulation in demersal
601 decapods at the VENUS cabled observatory in Saanich Inlet, British Columbia,
602 Canada. *J. Exp. Mar. Bio. Ecol.* **401**, 89–96. (doi:10.1016/j.jembe.2011.02.041)
- 603 60. Redmond, J. R. & Swanson, C. D. 1968 Preliminary studies of the physiology of the
604 Pycnogonida. *Antarct. J. United States* **3**, 130–131.
- 605 61. Markl, J. 1986 Evolution and Function of Structurally diverse Subunits in the
606 Respiratory Protein Hemocyanin from Arthropods. *Biol. Bull.* **171**, 90–115.
- 607 62. Douglas, E. L., Hedgpeth, J. W. & Hemmingsen, E. A. 1969 Oxygen consumption of
608 some Antarctic pycnogonids. *Antarct. J. United States* **4**, 109.
- 609 63. Tjonneland, A., Kland, S. & Nylund, A. 1987 Evolutionary aspects of the arthropod
610 heart. *Zool. Scr.* **16**, 167–175. (doi:10.1111/j.1463-6409.1987.tb00063.x)
- 611 64. Davenport, J., Blackstock, N., Davies, D. A. & Yarrington, M. 1987 Observations on
612 the physiology and integumentary structure of the Antarctic pycnogonid *Decolopoda*
613 *austratis*. *J. Zool.* **211**, 451–465.
- 614 65. Tjonneland, A., Kryvi, H., Ostnes, J. P. & Okland, S. 1985 The heart ultrastructure in
615 two species of pycnogonids, and its phylogenetic implications. *Zool. Scr.* **14**, 215–219.
616 (doi:10.1111/j.1463-6409.1985.tb00191.x)
- 617 66. Dresco-Derouet, L. 1978 Métabolisme respiratoire de *Nymphon gracile* Leach et
618 d'*Endeis spinosa* (Montagu) (Pycnogonida). *Cah. Biol. Mar.* **19**, 309–315.
- 619 67. Bates, A. E., Lee, R. W., Tunnicliffe, V. & Lamare, M. D. 2010 Deep-sea
620 hydrothermal vent animals seek cool fluids in a highly variable thermal environment.
621 *Nat. Commun.* **1**, 1–14. (doi:10.1038/ncomms1014)
- 622 68. Cannon, G. A. & Pashinski, D. J. 1997 Variations in mean currents affecting
623 hydrothermal plumes on the Juan de Fuca Ridge. *J. Geophys. Res.* **102**, 24,965–24,976.
- 624 69. Xu, G., Jackson, D. R., Bemis, K. G. & Rona, P. A. 2013 Observations of the volume
625 flux of a seafloor hydrothermal plume using an acoustic imaging sonar. *Geochemistry,*
626 *Geophys. Geosystems* **14**, 2369–2382.

627 70. Lowrey, P. L. & Takahashi, J. S. 2004 Mammalian circadian biology: elucidating
628 genome-wide levels of temporal organization. *Annu. Rev. Genomics Hum. Genet.* **5**,
629 407–441. (doi:10.1146/annurev.genom.5.061903.175925)

630

631 **Data accessibility**

632 The raw data used in this research have been made publically available on Ocean Networks
633 Canada: <http://www.oceannetworks.ca>.

634

635 **Competing interests**

636 We have no competing interests.

637

638 **Authors' contributions**

639 P.M.S., J.S. and R.L. designed the research project and developed the instrumentation. Y.L.,
640 P.L., M.M., S.M. P.M.S and J.S. conceived the ideas and contributed to the interpretation of
641 the results. Y.L. collected and analysed data. S.M. analysed and interpreted environmental
642 data. P.L. provided advice about the methods of statistical analysis. C.A. provided assistance
643 in the interpretation of Ammonoidea pycnogonid behaviour. P.L., M.M. and J.S. supervised
644 the research project. All authors assisted in the writing process and revised the manuscript.

645

646 **Funding statement**

647 This research was supported by a Natural Sciences and Engineering Research Council of
648 Canada (NSERC) research grant to P.L.

649

650 **Acknowledgments**

651 The authors thank the engineers and technicians who developed and maintain TEMPO-mini
652 (Ifremer RDT, LEP, ONC). Extended thanks go to the captain and crews of the R/V Thomas
653 G. Thompson, the staff of ONC and ROVs ROPOS and Oceaneering Millennium during the
654 deployment and recovery cruises. We are grateful to all PIs of ONC for accessing their
655 temporal data. This work was supported by the "Laboratoire d'Excellence" LabexMER
656 (ANR-10-LABX-19) and co-funded by a grant from the French government under the

657 program "Investissements d'avenir". We are also grateful to M. Lelièvre, L. Corbari (MNHN,
658 France) and the Québec Centre for Biodiversity Science.

659

660 **Figure legends**

661 **Fig. 1.** (A) Location map of the Main Endeavour Field (Juan de Fuca Ridge, Northeast
662 Pacific) indicating the positions of hydrothermal vents edifices, with (B) a visualization of the
663 topographic structure of Grotto. The yellow dot on Grotto represents the position of TEMPO-
664 mini. The distances and height were estimated from COVIS (Cabled Observatory Vent-
665 Imaging Sonar). (C) Deployed instruments: A = Remote Access Sampler (RAS);
666 B = assemblage filmed by TEMPO-mini camera; C = Benthic And Resistivity Sensors
667 (BARS); D = Aanderaa optode; E = TEMPO-mini ecological module; F = thermistor chain
668 (T-chain) and G = autonomous temperature loggers (F-probes).

669

670 **Fig. 2.** Normalised spectra of measured environmental variables with identified periodicity
671 bands. Degrees of freedom used to generate the spectra ranged from 24 to 98 based on length
672 of time series and resolution.

673

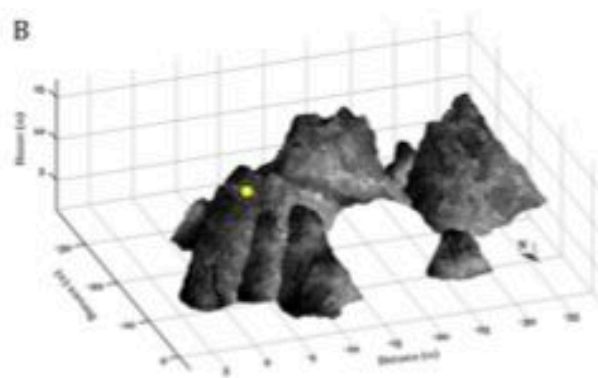
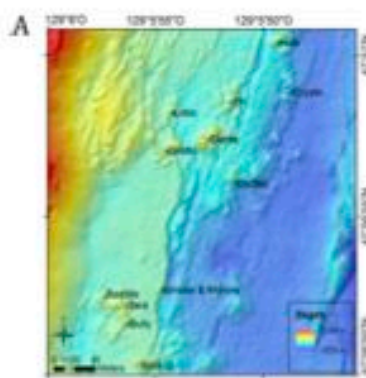
674 **Fig. 3.** Path analysis model of ocean tide effects on macrofaunal abundance for one summer
675 (June 2014) and two winter months (November and December 2014). Arrow colour indicates
676 the direction of the effect (black, positive; red, negative). Path coefficients indicate the direct
677 relationships between the different variables and their significance. Significance codes: no
678 significance (ns), (*) $p \leq 0.05$, (**) $p \leq 0.01$ and (***) $p \leq 0.001$. Indirect effects are
679 estimated by multiplying the coefficients of individual segments along paths. The percentages
680 shown in ellipses indicate the proportions of variance explained by the model (adjusted R^2).

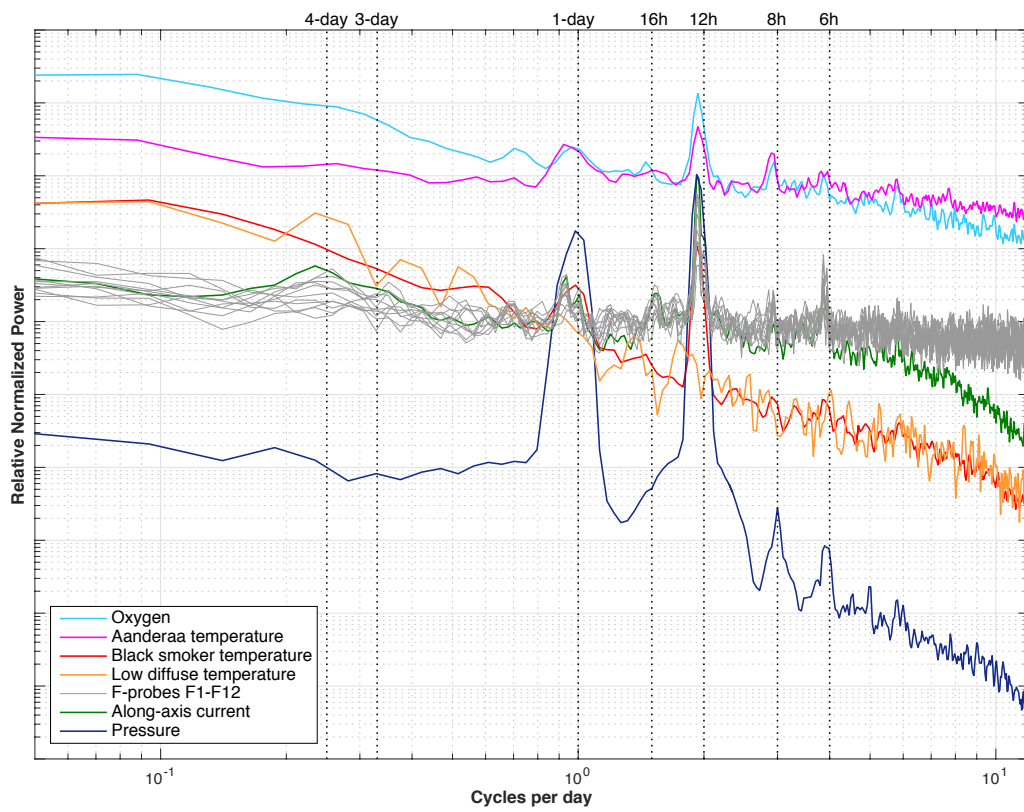
681

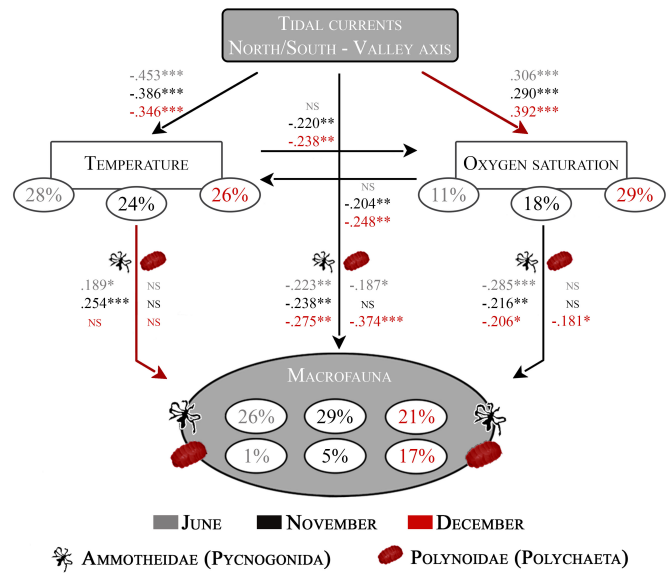
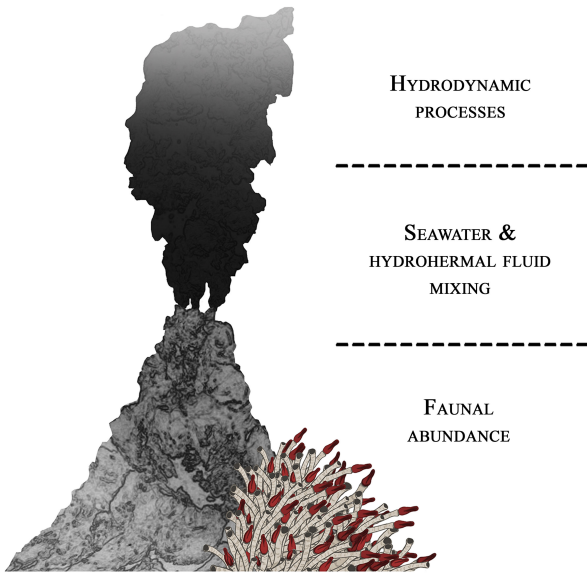
682 **Fig. 4.** Schematic representation of tidal and atmospheric forcing on habitat conditions and
683 vent species dynamics. The influence of ocean tides on the observed Ammotheidae
684 abundances followed a 12.4 h cycle (all study periods). In contrast, the effect on observed
685 Polynoidae abundances was felt only during December 2014. In November 2014, observed
686 abundances were additionally impacted by local surface storms with a 4-day (Ammotheidae)
687 and 16 h (Polynoidae) response, respectively. Current variability affects the balance between
688 hydrothermal fluid inputs and the surrounding seawater, modifying the physical and chemical
689 conditions of vent habitat. Hydrothermal species react to these habitat modifications by
690 adjusting their behaviour that is by moving up and down the tubeworm assemblage.

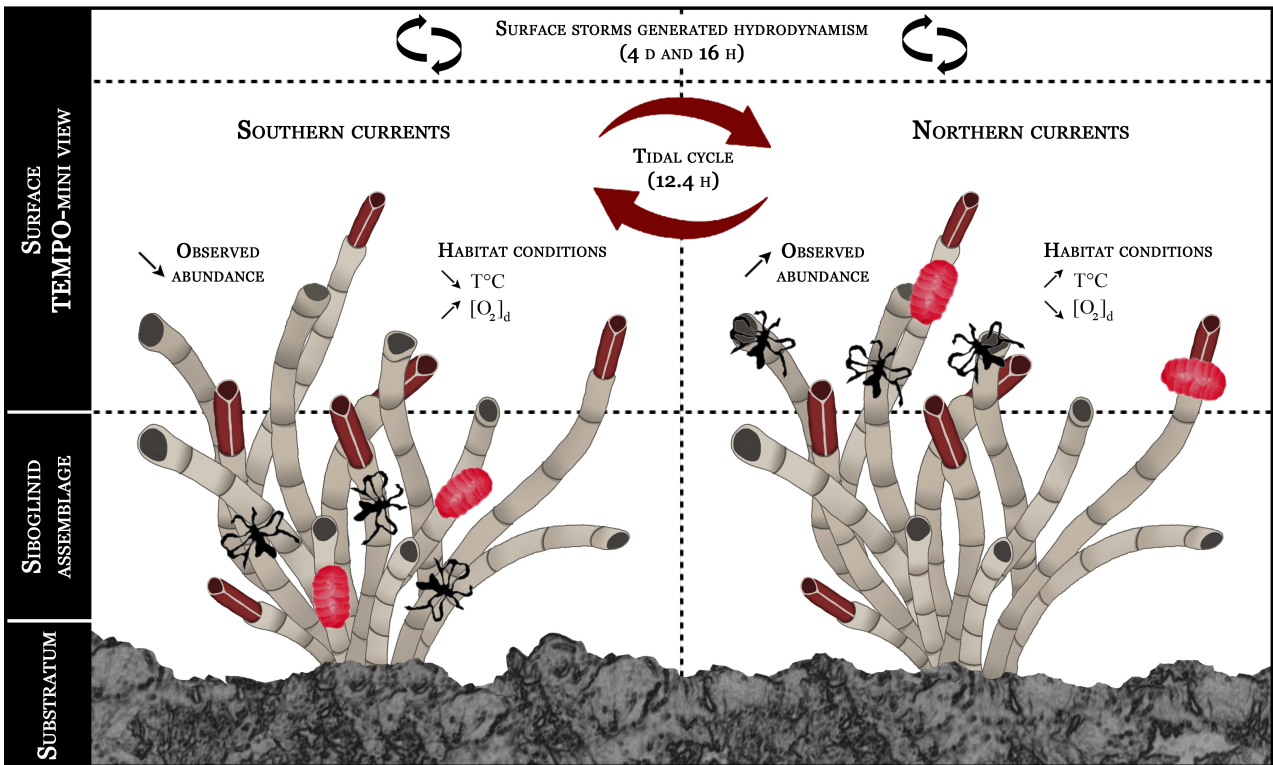
691

692 **Fig. 5.** Surface wind stresses and wave heights in the Northeast Pacific during 2014. These
693 components were used as indicators of storm activity. Shadowed parts in the graphics
694 correspond to the monthly faunal observations analyzed in this study.



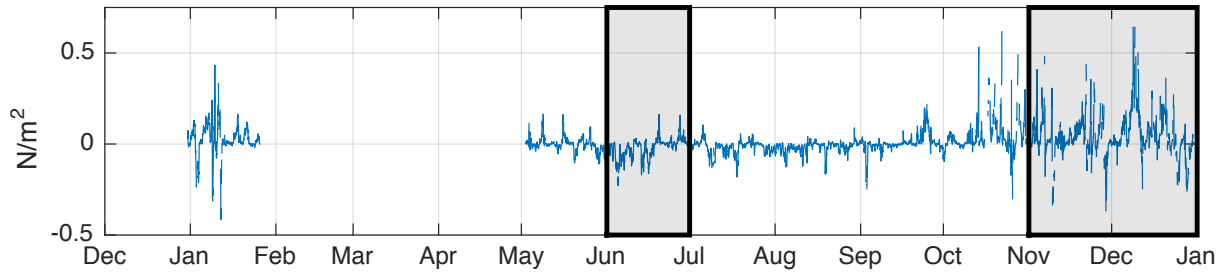




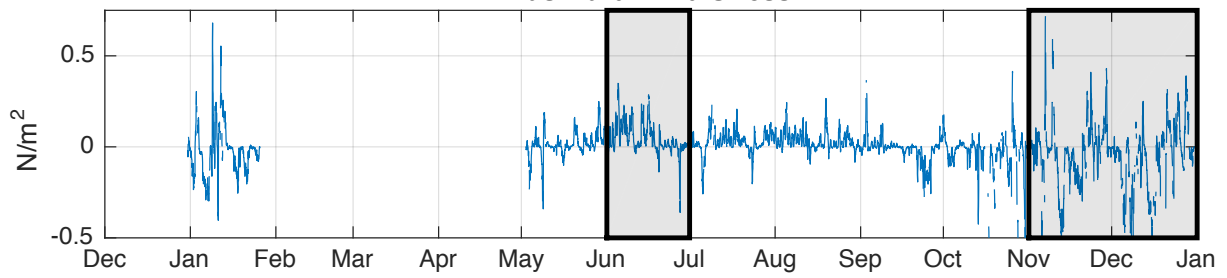


La Perouse Bank Meteorological Buoy C46206

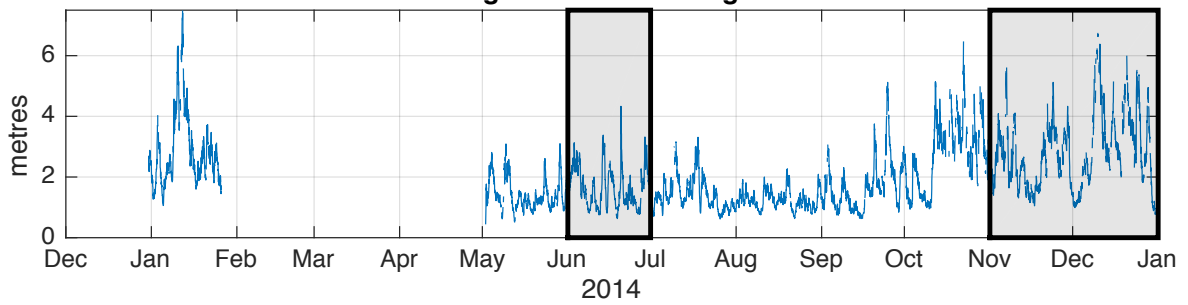
Northward Wind Stress



Eastward Wind Stress



Significant Wave Height



Supplementary Information for

Astronomical and atmospheric impacts on deep-sea hydrothermal vent invertebrates

Yann Lelièvre^{1,2*}, Pierre Legendre², Marjolaine Matabos¹, Steve Mihály³, Claudia P. Arango⁴,
Raymond W. Lee⁵, Pierre-Marie Sarradin¹, Jozée Sarrazin¹

¹*Institut Carnot Ifremer EDROME, Centre de Bretagne, REM/EEP, Laboratoire Environnement Profond, F-29280 Plouzané, France.* ²*Département de sciences biologiques, Université de Montréal, C.P. 6128, Succursale Centre-ville, Montréal, Québec, H3C 3J7, Canada.* ³*Ocean Networks Canada, University of Victoria, PO Box 1700 STN CSC, Victoria, BC V8W 2Y2, Canada.* ⁴*Biodiversity Program, Queensland Museum, PO BOX 3300 South Brisbane QLD 4101, Australia.* ⁵*School of Biological Sciences, Washington State University, Pullman, WA 99164, USA.*

correspondence to: yann.lelievre@ifremer.fr

This PDF file includes:

Supplementary Figure S1

Fig. S1. Phase relationships among the environmental variables.

Supplementary Table S1

Table S1. List of instruments used in this study, summarizing the characteristics, the habitat conditions as well as the periods for each variable of interest, and the principal investigators responsible for the instruments.

Supplementary Table S2

Table S2. Observed abundances and periodic analyses of the hydrothermal vent fauna at the Grotto edifice (2 196 m depth). Data are based on the manual analysis of video images recorded by the TEMPO-mini ecological module.

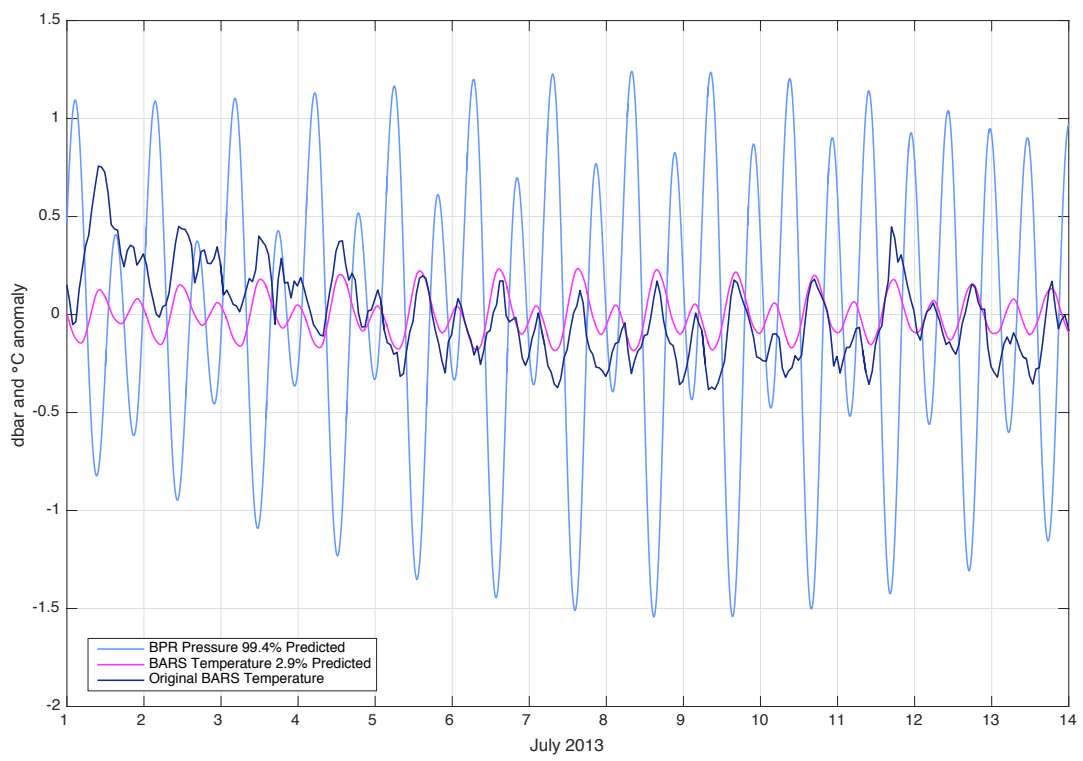


Table S1. List of instruments used in this study, summarizing the characteristics, the habitat conditions as well as the periods for each variable of interest, and the principal investigators responsible for the instruments.

Instruments (units)	Sample interval	Acquisition frequency	min-max (mean \pm sd)	Main periods	Principal Investigators
BPR (bar) <i>Bottom Pressure Recorder</i>	Pressure	1 second	220.03-222.69 (221.32 \pm 3.78)	3-4 day 12.4 h and 24.8 h	R.Thomson
ADCP (cm/s) <i>Acoustic Doppler Current Profiler</i>	Current	1 second	0.00-20.73 (4.99 \pm 2.83)	3-4 day 12.4 h and 24.8 h	S. Mihály
BARS (°C) <i>Benthic and Resistivity Sensors</i>	Temperature black smoker	20 seconds	330.43-334.7 (332.58 \pm 0.64)	12.4 h 24.8 h	M. Lilley
RAS (°C) <i>Remote Access Water Sampler</i>	Temperature diffuse flow	1 second	31.47-74.66 (45.71 \pm 5.76)	12.4 h 24.8 h	D. Butterfield
F-probes (°C) F1-F12	Temperature Siboglinidae assemblage	1 hour	1.6-13.6 (3.9 \pm 0.6)	12.4 h 24.8 h	R. Lee
Andearaa Optode Temperature (°C)	Temperature Siboglinidae assemblage	30 seconds	1.93-4.96 (2.7 \pm 0.32)	12.4 h 24.8 h	P-M. Sarradin
Andearaa Optode Oxygen (% saturation)	Oxygen Siboglinidae assemblage	15 minutes	1.53-22.07 (11.56 \pm 3.35)	12.4 h 24.8 h	P-M. Sarradin

Table S2. Observed abundances and periodic analyses of the hydrothermal vent fauna at the Grotto edifice (2 196 m depth). Data are based on the manual analysis of video images recorded by the TEMPO-mini ecological module.

Taxa	Annual analysis		Monthly analyses					
	2013-06-20 to 2014-06-20		June 2014		November 2014		December 2014	
	min-max (mean \pm sd)	Main periods	min-max (mean \pm sd)	Main periods	min-max (mean \pm sd)	Main periods	min-max (mean \pm sd)	Main periods
Ammotheidae	2-31 (14.7 \pm 5.85)	15 day	14-46 (24.32 \pm 5.62)	12.4 h	15-48 (26.75 \pm 5.57)	4 day 12.4 h	9-37 (23.65 \pm 5.36)	12.4 h
Polynoidae	1-34 (8.57 \pm 3.53)	-	4-20 (10.81 \pm 3.47)	-	7-24 (14.68 \pm 3.6)	16 h	7-25 (14.36 \pm 3.86)	12.4 h
Buccnidae	4-22 (12.2 \pm 3.13)	-	8-22 (14.99 \pm 2.56)	-	12-22 (17.12 \pm 2.19)	-	8-22 (15.16 \pm 2.73)	-
Zoarcidae	0-6 (1.66 \pm 1.22)	-	0-5 (1.42 \pm 1.05)	-	0-4 (0.74 \pm 0.85)	-	0-4 (0.92 \pm 0.96)	-